Talanta 120 (2014) 239–247

Contents lists available at ScienceDirect

Talanta

journal homepage: www.elsevier.com/locate/talanta

# Reliable classification of moving waste materials with LIBS in concrete recycling

Han Xia*, M.C.M. Bakker

*Delft University of Technology, Faculty of Civil Engineering and Geosciences, Resources and Recycling Group, Stevinweg 1, 2628 CN, The Netherlands*

ARTICLE INFO

*Article history:*
Received 5 July 2013
Received in revised form
22 November 2013
Accepted 28 November 2013
Available online 4 December 2013

*Keywords:*
LIBS
Recycling
Demolition concrete
Classification
PCA
PLS-DA
Adaboost

ABSTRACT

Effective discrimination between different waste materials is of paramount importance for inline quality inspection of recycle concrete aggregates from demolished buildings. The moving targeted materials in the concrete waste stream are wood, PVC, gypsum block, glass, brick, steel rebar, aggregate and cement paste. For each material, up to three different types were considered, while thirty particles of each material were selected. Proposed is a reliable classification methodology based on integration of the LIBS spectral emissions in a fixed time window, starting from the deployment of the laser shot. PLS-DA (multi class) and the hybrid combination PCA–Adaboost (binary class) were investigated as efficient classifiers. In addition, mean centre and auto scaling approaches were compared for both classifiers. Using 72 training spectra and 18 test spectra per material, each averaged by ten shots, only PLS-DA achieved full discrimination, and the mean centre approach made it slightly more robust. Continuing with PLS-DA, the relation between data averaging and convergence to 0.3% average error was investigated using 9-fold cross-validations. Single-shot PLS-DA presented the highest challenge and most desirable methodology, which converged with 59 PC. The degree of success in practical testing will depend on the quality of the training set and the implications of the possibly remaining false positives.



## 1. Introduction

Laser induced breakdown spectroscopy (LIBS) is an optical technique using a pulsed laser to produce a high power density light beam to sample tiny amounts of material from the surface of the target material. The sampled material is ablated to form a hot ionised gas (the plume), which emits the observable spectra. The spectra depend on the laser type and on a chain of physical processes and parameters related to the target material, ablation, plume dynamics and ambient conditions in which the plume is produced [1–4]. This combination of complex transient processes is the reason why the physics of LIBS is not yet fully understood and the subject of continuing investigation.

The stand-off capability, relative simplicity in instrumentation, ease of use and ability to detect a wide range of elements has made LIBS a popular choice for inspecting materials such as polymers [5–7], metal scrap [8], automobile catalyst [9], and wood [10]. LIBS has also been investigated for building maintenance, such as on-site assessment of chlorines in concrete [11] and fast chemical mapping of concrete surfaces [12]. Quantitative LIBS was used for measuring the elemental composition of recycle concrete particles [13].

The main challenge in the upgrading of recycle concrete to new concrete is to safeguard quality. Demolition concrete will to some degree be polluted with all kinds of building materials found in domestic dwellings. The most common pollutants are wood, brick, plastics, gypsum block, glass, and metals, which can all be detrimental for the quality of the new concrete. These waste particles have a particle size range of 2–32 mm and are transported on conveyor belts, typically at 30 cm/s. For the envisioned inline application above the conveyor, it is preferable to operate the laser in free air to reduce laser setup complexity and maintenance costs.

The free air poses a challenge to the detection of non-metals such as C, S, Cl for several reasons. First, the targeted non-metals have high excitation energies ( $>10$ eV) and generally show low emissivity. Second, the dominant emission lines are in the deep-UV and NIR ranges, e.g., C 247 nm, S 921 nm, Cl 837 nm, which wavelengths are susceptible to absorption by oxygen (UV) and water vapour (NIR). Third, the laser beam gives rise to localised air breakdown [14], often initiated by tiny specks of dust. Consequently, emissions from ionised air elements such as H, C, N and O may interfere with those from the target material. Additionally, the reactions between the ionised plume and the ambient air appear to reduce the life time of the emission spectrum and the obtainable signal levels [15]. More costly methods for improvement on these three points would be to use an inert gas for flushing the optical path, or sustaining the vacuum along most of the optical path, or using more sensitive detectors such as ICCD.

* Corresponding author.Tel: +31 (0)152781473.
*E-mail addresses:* h.xia@tudelft.nl, xhtp2008@hotmail.com (H. Xia), m.c.m.bakker@tudelft.nl (M.C.M. Bakker).

0039-9140/$ - see front matter © 2013 Elsevier B.V. All rights reserved.
http://dx.doi.org/10.1016/j.talanta.2013.11.082

Yet another challenge is the large dynamic range in the LIBS spectra. For example, alkali rich materials are overly sensitive to LIBS and their emissions commonly dominate the spectrum [16]. This may lead to poor signal-to-noise ratios for the far less sensitive minor elements, which are often of main interest for identification and quantitative analysis. Moreover, if saturation occurs the blooming effect of the CCD may obscure adjacent emission lines.

Due to the material-specific conditioning procedures, quantitative LIBS cannot reliably deliver the information required for quality assessment of a moving stream of different waste materials [17]. Instead, proposed is to develop a classification methodology that employs all the physical information delivered by the LIBS experiment. To this end, the time-window of integration starts at the moment of laser pulse deployment and finishes after 10 μs. This fixed time-window produces spectra that contain information about all stages of the LIBS experiment, which is from the moment of ablation up to the condensation of molecules in the ionised plume. The fixed time window avoids the usual tuning of the start and duration of the time window of integration for each material, which makes quantitative LIBS material-sensitive. The approach neither requires any processing to eliminate continuous emissions, nor does it require the material sensitive calibration procedures of the quantitative LIBS methods. This combination of properties makes the proposed LIBS methodology also less sensitive to the disturbing emissions experienced when operating in free air.

The unknown spectra need to be classified for which we selected the supervised methods partial least-square discriminant analysis (PLS-DA) and principal component analysis coupled with adaptive boosting algorithm (PCA–Adaboost). PCA has to be complemented by another algorithm to obtain the classification, for which binary adaptive boosting (Adaboost) is chosen as the most suitable in a one-against-all approach. Adaboost is once claimed to be the best off-the-shelf binary classifier in the world [18], and has been employed for near-infra red spectra [19], but has not been applied to LIBS spectra before. We investigate and compare the capabilities of the hybrid PCA–Adaboost method and PLS-DA, while also comparing mean centre and auto scaling approaches for both classifiers. Subsequently, we investigate the effects of a reduction in data averaging up to the single-shot scenario as the ultimate real-time methodology for detecting moving waste materials.

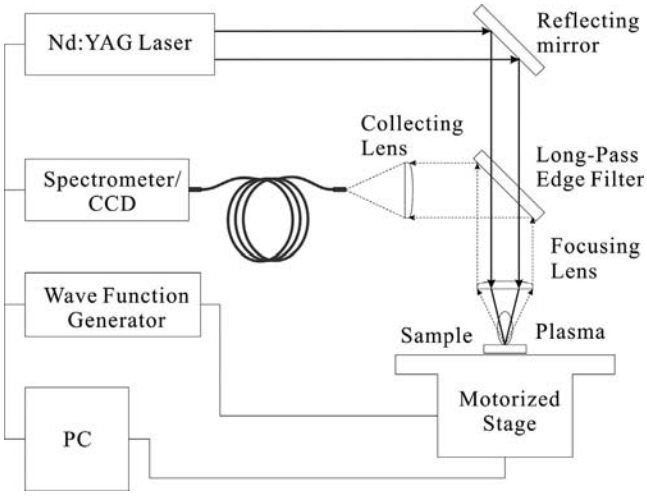


**Fig. 1.** The LIBS setup.

## 2. Methods and materials

### 2.1. Experimental setup and data processing

The laser in Fig. 1 is a 1064 nm diode pumped, Q-switched Nd: YAG (Quantel Centurion), which delivers a 25.7 mJ pulse in 6.9 ns with a maximum repetition rate of 100 Hz. It is noted that in industrial operations a diode pumped laser is far preferable to a flash lamp laser in view of the levels of maintenance and risk for process continuity. The laser should be operated 60 h/week at 100 Hz, with the consequence that a diode pumped laser pack typically needs replacement every 46 weeks ($10^9$ shots), while a flash lamp would need replacement twice a week ($10^7$ shots). The laser beam in Fig. 1 is folded by the reflecting mirror and focused onto the sample surface by a plano-convex lens of 50 mm focal length ($f/4$). This gives a power density of 21 GW/cm$^2$ on a 150 μm diameter spot, which is some hundred times higher than that needed for breakdown of metals [20].

The emitted light propagating anti-parallel to the incident laser beam is collected by the lens and folded by a long pass edge filter (800 nm cut-off) that is transparent to the infrared laser light. A second plano-convex lens is placed behind the filter to focus the incoming light on the entrance of a bundle of seven optical silica fibres. The receiving end of the fibres is coupled to a Czerny–Turner spectrometer with bandwidth 250–800 nm, focal length 75 mm and 3648 pixels CCD. This results in a resolution of 0.32 nm (FWHM). The simultaneous triggering of the laser unit and spectrometer is performed by an external pulse generator. Light collection starts at the moment the laser pulse is applied and ends after 10 μs. A longer integration time did not noticeably contribute to the quality of the spectra but it did increase the chance of saturation. The raw spectra $D(\lambda)$ are first averaged over N shots and then normalised to the spectral integral, which strongly suppresses shot-to-shot variability to help develop the optimum classification methodology

$$S^{AVG}(\lambda) = \left[\int_{250\ nm}^{800\ nm} \left(\sum_{n=1}^{N} D_n(\lambda)\right) d\lambda\right]^{-1} \sum_{n=1}^{N} D_n(\lambda) \quad (1)$$

Samples were moved at a constant speed of 30 cm/s to simulate materials transport on a typical feed conveyor belt. At 100 Hz the laser would sample every 3 mm of the waste stream. It is noted that the quality of the LIBS spectra was stable for material transport velocities up to 3 m/s.

### 2.2. Samples

For each material, thirty different particles were randomly selected from streams of demolition concrete to represent the material and material types (cf. Fig. 2): cement (CEM I 42.5 R HS, CEM II/B-S 52.5 N, CEM III/B 32.5 N), brick (yellow, brown and red), gypsum block (white, blue and red), wood (pine, ash and walnut), PVC plastic (grey, black pipe and grey hard plate), glass (white, green and brown), two of the most common types of aggregate (sandstone and gabbro) and steel rebar, of which only one type is used in the Netherlands. Each set of thirty particles were evenly divided between the different types to form a total samples set of two hundred forty particles.

Compressed air was used to clean the dust from the waste particles, which is also quite feasible when the materials are in transport on a conveyor belt. In fact, it may be preferable to the alternatives, such as using a more powerful laser (requiring flash lamps) or using two lasers where one fires first to clean the surface. In the envisioned application, the moving feed layer of 2–32 mm concrete waste particles will be scraped off continuously

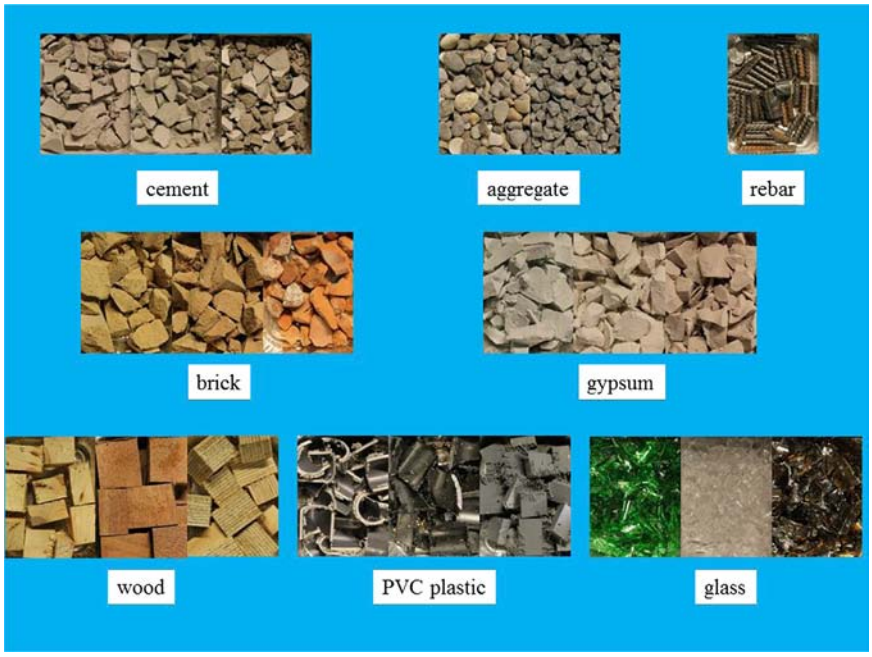


**Fig. 2.** Eight waste materials and selected types from a stream of demolition concrete.

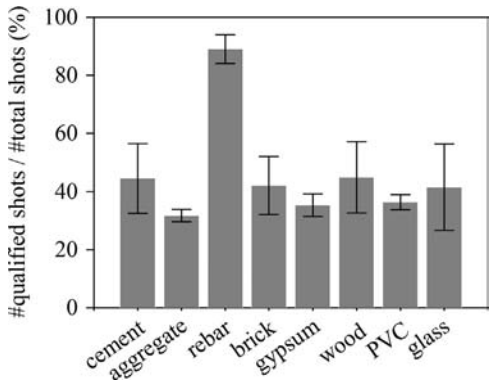


**Fig. 3.** The qualified spectra as a percentage of the total number of deployed laser shots. The bar shows the mean for the thirty particles per waste material, and the brackets show the standard deviation.

to provide a flattened material surface level for the laser to focus on. This avoids the need for an autofocus unit. To simulate the scraping effect, the tops of the nine waste particles were roughly levelled on the rotating plate using double-sided tape. In our setup, six particles were mounted at a time, rotated and sampled until thirty acceptable (qualified) single-shot spectra per particle were acquired. This process was repeated forty times for the total of two hundred forty particles. Data qualification was applied, where the non-qualified spectra were too much distorted by shot-to-shot variations due to different lens-to-particle distances and laser-material interaction conditions. To that end, upper and lower limits for the maxima of a spectrum were set, corresponding to 98% and 42% of the dynamic range of the detector, to eliminate the saturated and otherwise poor spectra. Fig. 3 shows how many shots are required for each material to obtain the thirty qualified spectra. For most materials between 30% and 45% of all shots are qualified. This means that in practice in a single-shot scenario one would need at least three–four shots per particle to obtain at least one qualified shot. The non-qualified ones may mostly be attributed to misses (particle spacing), particle edges, surface roughness and porosity, material heterogeneity and high transparency in case of glass. The steel rebar was quite uniform in material, shape and size, which contributed to the high percentage of qualified spectra.

The type of cement in concrete demolition waste is of minor interest in the present work, because the focus is on detecting the waste pollutants. It should also be pointed out that cement stone from demolished concrete is in fact a mixture of sand and cement, where the sand has a similar geological origin as the concrete aggregate. Of the waste metals only steel rebar is selected, because other building metals (e.g., aluminium) proved just as easy to discriminate from other waste types as steel. From the large variety of rock types used for concrete aggregate, sandstone and gabbro are arguably the most widely used sources. To emphasise the cement properties instead of the concrete sand, three types of pure cement paste were prepared by mixing cement powder and distilled water to a water/cement ratio of 0.5. It was left to cure for several days to its full strength and was then broken up into particles.

## 3. Results

### 3.1. LIBS spectra

LIBS photonic emissions are primarily produced by the ionised plume, though some emissions may be expected from air molecules interacting with the plume and from the hot ablated sample surface. The plume is the result of a sequence of complex physical processes, active during overlapping stages from initiation to extinction of the LIBS experiment [21]. In particular, the optical absorption of laser light, dielectric breakdown, heating, melting, ablation and shock wave formation, the stages of plume expansion and plume reheating by absorption of part of the laser energy [22]. As a result, the produced emissions may be linked to quite different physical processes. To simplify matters we distinguish three types of detectable emissions: continuous radiation, ionic–atomic emissions and emission bands.

Continuous radiation spans a wide range of wavelengths, linked to as many available energy transitions from ionised species and electrons, e.g., free–free and free-bound transitions [23]. These

transitions can occur as long as the plume is optically dense and ionised. However, the observed radiation spectra may be quite different for different types of material. This implies that the possible energy transitions and/or most probable emissions depend on the species and degree of ionisation of the plume, which in turn are determined by the target material and the effectiveness of the ablation process.

The emission bands arise both in the hottest stage, e.g., Stark broadening and fluorescence shifts, as well as after some cooling down of the plume when molecules can start forming. The emission bands are also expected to be highly dependent on the composition of the original target material, how much material is effectively ablated and how hot the plume becomes, and how this particular mix of ionised species eventually condenses.

Complex as the processes may be, the continuous radiation and emission or absorption bands may quite well be carrying discriminating information on the target material composition and, quite likely, the specific way in which it influenced the ablation process. This means these spectral contributions may be utilised for materials discrimination, even though it is (as yet) not physically tractable and is therefore probably of little use for quantitative measurements. The ionic–atomic emissions are physically tractable and may, if conditions and calibrations permit it, be used to quantify the elemental concentrations in the target material.

In view of the diversity of potential physical information, it was the logical decision to collect all the types of spectral emission delivered by the LIBS experiment and let the classification algorithms extract the discriminating information. This way, we also avoid the material sensitive calibration procedures and tuning of the time integration window.

Fig. 4 shows the representative spectra for the waste materials and indicates a few characteristic emission lines and bands. The discriminating emission lines in PVC are Cl (594 nm), CaCl bands (618 nm), CN bands (387 nm) and Ca (422 nm). It indicates the presence of $CaCO_3$, which is a common type of filler in thermoplastics. Since wood is principally made up of cellulose and lignin, the CN, H, O emission lines were already expected to be quite apparent. Due to the porosity of wood, the laser energy was more prone to be absorbed by air pockets and the spectrum therefore shows strong N emissions. The spectrum of glass shows the expected elements Ca and Si, but it also indicates the presence of Ba as an inherently toxic element. The rebar shows multiple, well resolved Fe-related emission lines. The gypsum block shows only very weak evidence of S in the 550–556 nm range, while the elemental S content in the gypsum block is estimated as 15 wt%.

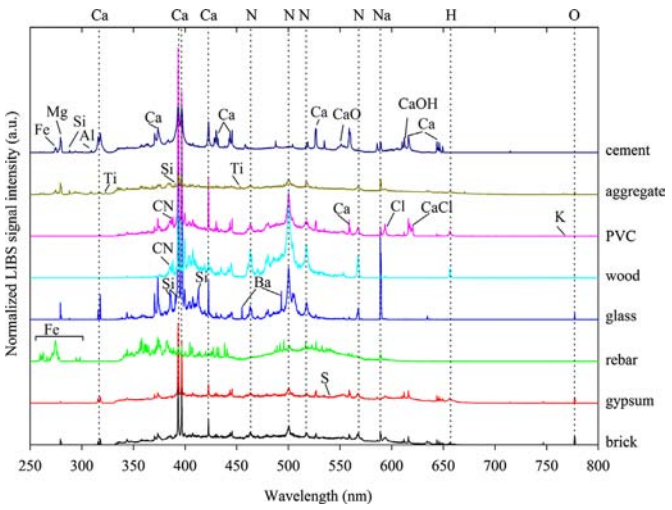


**Fig. 4.** Normalised LIBS spectra for eight building waste materials.

The brick and cement show a similar composition as gypsum block in the elements Ca, Si, Al, Fe, Mg and Na. The reason is the presence of clay, also the main component of brick, which is fed together with lime into the cement kiln to produce the clinker. It is noted that gypsum is also an additive in cement and improves the setting properties of the fresh mortar. The CaO and CaOH bands were easiest to observe in cement due to its higher Ca content. The continuum contribution to the spectrum appears relatively stronger for the mechanically harder and optically opaque types of material. In this work those are steel rebar, concrete aggregates and cement, where it is reminded that the presented spectra are normalised according to Eq. (1). It may be inferred from these comparisons that the LIBS spectra are also sensitive to the optical and mechanical properties of the target materials by virtue of the underlying laser absorption and ablation processes. Judging from the fact that sometimes the most characterising element emissions are weak or even absent for some waste materials, e.g., sulphur in gypsum block, the complete time history provided by LIBS should be utilised to improve the reliability of the classification methodology.

### 3.2. PLS-DA

PLS-DA requires a training session before it can be applied to unknown data, which (supposedly) fall within the variance of the training data. In training, $X$ denotes the predictor matrix with known spectra of the eight different waste materials. The raw spectra were averaged over ten shots and normalised according to Eq. (1). Then, mean centre and auto scaling approaches were applied and compared. In mean centre the column mean is set to zero for both $X$ and $Y$ matrices and the spectral variation is used instead of absolute values. In auto scaling the column mean is also set to zero, but in addition the column standard deviations are set to unity. Therefore, auto scaling gives the same weight to all wavelengths. This enhances the role of small emission peaks, but noise may also become more pronounced.

With 72 spectra (10 averaged) per material, a $576 \times 3648$ predictor matrix is obtained. Corresponding to $X$, the response variable $Y$ is a $576 \times 8$ label matrix which classifies the materials either as a one (target material, one against all) or as a zero (other material). PLS regression will solve for the prescribed number of principal components (PC) by utilising the correlation between $X$ and $Y$, after which the PC that contribute most to the correlation in the system of equations are selected to span a reduced space to represent the correlated multivariable data. In this work we used the "plsregress" function from Matlab 2012b, which is based on the SIMPLS algorithm [24]. The training session yields an output correlation coefficient matrix between $X$ and $Y$, which during operation should be multiplied with an unknown test spectrum to determine the class. The unknown spectrum is assigned to the class for which the calculated $Y$ value is closest to unity.

The number of PC is a primary parameter in PLS-DA. Selecting too few could result in under-fitting, while too many could result in significant over-fitting in the calibration model. Whereas over-fitting may improve the training, the prediction performance during testing may be poor. Usually, the number of PC is chosen by examining the percentage of variance explained by the model and the relative mean squared error of cross-validation (RMSECV).

With the 9-fold cross-validation the training dataset was partitioned into nine mutually exclusive and equal subsets. Each subset was used as a test set, while a PLS model was trained using the other subsets. The nine results were averaged to produce a single PLS calibration model. This internal validation method makes it possible that each sample may be seen as a testing

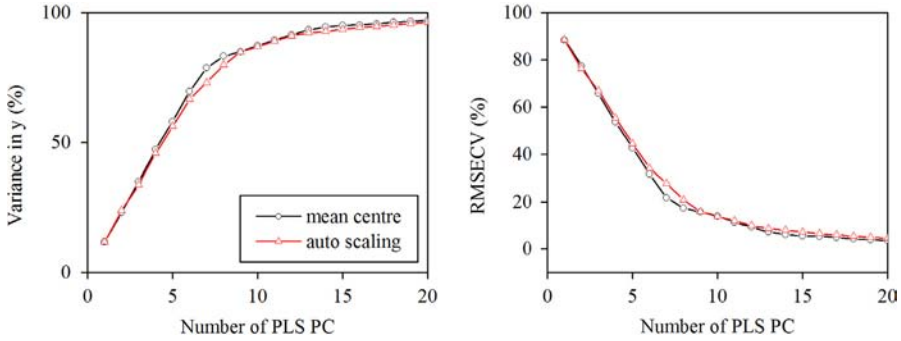


**Fig. 5.** Variance explained in the response variable as a function of the number of PLS PC (left) and the RMSECV for 9-fold cross-validation (right) using mean centre and auto scaling.

**Table 1**
Misclassification rates of PLS-DA (with mean centre) during training for increasing number of PC. For each material 72 training spectra were used.

| #PC | Cement | Aggregate | Rebar | Brick | Gypsum | Wood | PVC | Glass |
|---|---|---|---|---|---|---|---|---|
| 1 | 0.0 | 100.0 | 100.0 | 100.0 | 100.0 | 0.0 | 100.0 | 100.0 |
| 2 | 0.0 | 100.0 | 0.0 | 100.0 | 95.8 | 1.4 | 100.0 | 0.0 |
| 3 | 0.0 | 100.0 | 0.0 | 16.7 | 27.8 | 0.0 | 100.0 | 0.0 |
| 4 | 6.9 | 58.3 | 0.0 | 0.0 | 0.0 | 0.0 | 100.0 | 0.0 |
| 5 | 9.7 | 97.2 | 0.0 | 0.0 | 0.0 | 0.0 | 16.7 | 0.0 |
| 6 | 9.7 | 15.3 | 0.0 | 11.1 | 0.0 | 0.0 | 16.7 | 0.0 |
| 7 | 6.9 | 12.5 | 0.0 | 11.1 | 0.0 | 0.0 | 16.7 | 0.0 |
| 8 | 5.6 | 5.6 | 2.8 | 0.0 | 0.0 | 0.0 | 16.7 | 0.0 |
| 9 | 5.6 | 1.4 | 0.0 | 0.0 | 0.0 | 0.0 | 16.7 | 0.0 |
| 10 | 0.0 | 1.4 | 0.0 | 0.0 | 0.0 | 0.0 | 16.7 | 0.0 |
| 11 | 0.0 | 0.0 | 0.0 | 0.0 | 0.0 | 0.0 | 16.7 | 0.0 |
| 12 | 0.0 | 0.0 | 0.0 | 0.0 | 0.0 | 0.0 | 16.7 | 0.0 |
| 13 | 0.0 | 0.0 | 0.0 | 0.0 | 0.0 | 0.0 | 8.3 | 0.0 |
| 14 | 0.0 | 0.0 | 0.0 | 0.0 | 0.0 | 0.0 | 1.4 | 0.0 |
| 15 | 0.0 | 0.0 | 0.0 | 0.0 | 0.0 | 0.0 | 0.0 | 0.0 |

instance for which the prediction error (RMSECV) can be calculated. Therefore, the resultant model using cross-validation could be more representative for the statistical spreading of the data than, for example, goodness of fit that depends significantly on the choice of training dataset.

Traditionally, the number of PC is determined by the point where the RMSECV is minimal. In this case, the RMSECV estimate for a 9-fold cross-validation reaches a local minimum for both mean centre (1.5% of RMSECV and 99.8% variance in *Y*) and auto scaling (2.0% of RMSECV and 99.6% variance in *Y*) with the first 59 PC. Mean centre performs slightly better as it shows a higher variance in *Y* and a lower RMSECV. However, both methods (cf. Fig. 5) converge very slowly after 17 PC and the RMSECV is less than 5% using mean centre. We choose mean centre for PLS in the remainder of this work.

Cross-validation is mostly applied in quantitative calibrations, because the error can be accurately calculated as a continuous value. However, cross-validation can overestimate the number of PC required for classification since the classification rules may exaggerate the error. Table 1 shows the misclassification rate for increasing PC during training, based on 72 spectra of each material. This approach is also known as "goodness of fit". In contrast to the 59 PC determined using 9-fold cross-validation, only 15 PC are shown to provide full classification during training, corresponding to a RMSECV of 5.5%. PVC proves to be the most challenging.

It is desirable to find a reliable relation between the number of PC as determined by 9-fold cross-validation and goodness of fit. To this end, 18 testing spectra per material are used in two PLS models, which results are compared in Fig. 6. Six glass test spectra were misclassified as brick (4), aggregate (1) and gypsum (1),

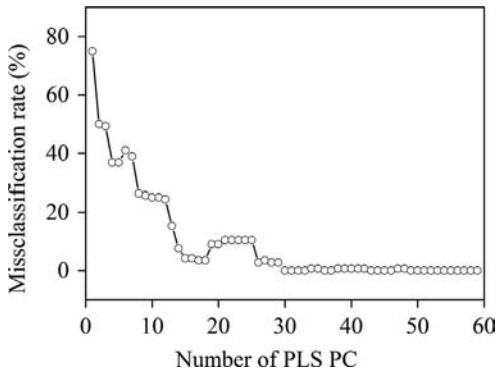


**Fig. 6.** Misclassification rate (ratio of misclassified to total number of test spectra).

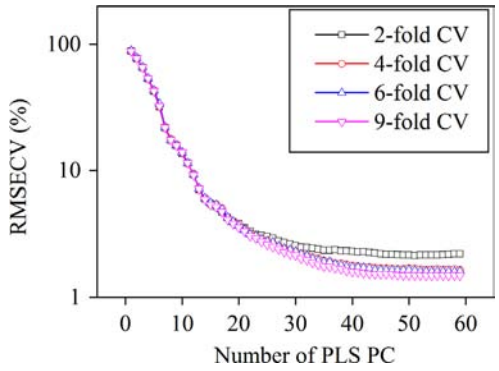


**Fig. 7.** RMSECV with increasing number of PLS PC applying different folds of cross-validation in semi-logarithm.

using a parsimonious PLS model with 15 PC. Apparently, this error is the result of under-fitting. In this case, addition of PC may help cover a possibly wider spread during testing. With 59 PC, all 18 spectra for each material are fully classified and hence, not over-fitted.

Fig. 6 shows that full classification is achieved for the first time with 30 PC, corresponding to 2.2% of RMSECV. However, with increasing PC, the curve fluctuates until it remains zero at 49 PC (1.5% of RMSCV). This level of correspondence between cross-validation and goodness of fit might vary according to the partition of training and testing datasets. In this sense, cross-validation appears more reliable, even though it introduces here some 10 redundant PC.

To gain same insights into the influence of partition of datasets on PLS performance, 2, 4, 6, 9-fold cross-validation (corresponding to 1, 3, 5 and 8 training to testing datasets ratios) were employed to evaluate RMSECV for increasing PC in Fig. 7. The main

differences were observed for higher numbers of PC. With relatively large training sets the RMSE values are lower, indicating a better classification at the cost of using more PC. It appears a compromise should be made between the number of training samples and the misclassification rate. It is noted that the RMSECV cannot be lower than 2% if the training set is smaller than the testing set. Practically, the PLS algorithm did not converge for all numbers of PC. Fig. 7 shows that up to 20 PC the convergence rate does not depend on the relative size of the training set. For more than 30 PC, the convergence rate reduces to a crawl, indicating increasing uncertainty in how many PC will be required for full discrimination.

### 3.3. PCA–Adaboost

Principal component analysis (PCA), like PLS, aims to find a reduced space to represent the correlated multivariable raw spectra. The method is different from PLS in that it aims to maximise the contribution to the variance of first few PCs in the *X* matrix and is a non-supervised method by which it does not perform classification. For the latter purpose the PC are fed to an adaptive boosting algorithm [25]. PCA–Adaboost requires a training session before it can be applied to unknown spectra. The *X* and *Y* input data were pre-processed similar as for PLS-DA and fed to the PCA algorithm "princomp" of Matlab 2012b. For training, PCA created a $3648 \times K$ loading matrix and a $576 \times K$ score matrix. The score matrix and a 567 label vector (1 for target material and $-1$ for the rest) were fed to the Adaboost algorithm using the STPRTool [26] to build the classification model. A binary weak classifier on each PC score was used to determine the misclassification error. Adaboost first picks up the weak classifier/PC score with minimum misclassification error ( $>50\%$ predictability), then gives more weight to the misclassified data, and finds the second weak classifier/PC score, possibly the previous one. This process is repeated until all the weak classifiers combine to a strong classifier. The only tuneable parameter is the number of iterations. We explored the hybrid PCA–Adaboost model by investigating the weighted error (error for single weak classifier) and error bound (error for the combined classifier). The weighted error evaluates the total performance of the model and the error bound stops the iteration. The classification rule during testing is the same as for PLS-DA. Details on Adaboost and binary weak classifiers may be found in literature [19,25].

Fig. 8 shows PCA clusters for the eight waste materials using the first two PC scores with mean centre (Fig. 8a) and auto scaling (Fig. 8b), accounting for 83% and 69% of the total variance, respectively. They reveal nicely distinct clusters, regardless of the scales of the PC scores and the direction of the PC1 axis. Glass overlaps with aggregate, while wood, PVC and rebar are already well isolated. Cement was better isolated from brick using auto scaling.

The PCA scree plot Fig. 9 shows that the first five PC account for more than 95% of the cumulative variance in *X*. Mean centre converges faster than auto scaling, since in auto scaling the noise plays a relatively more pronounced role.

Adaboost is employed to determine classes from the PCA-PC scores. A few other linear classifiers, reported to be little susceptible to over-fitting, were also tested. The unsupervised types proved less effective, such as *K*-mean clustering (multi class) and Fischer linear discriminant (binary class). Of the supervised classifiers, Perceptron (multiclass) may perform well for sufficiently resolved classes but it could not find a satisfactory boundary in case of overlapping clusters, similar to the case for cement and brick in Fig. 8a.

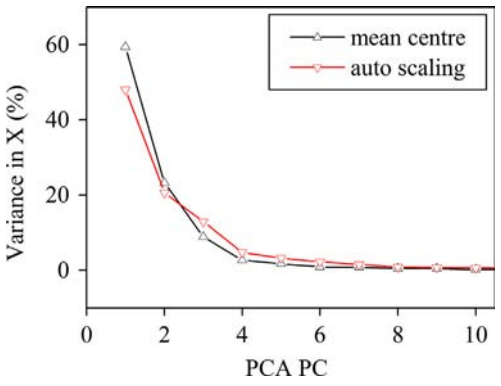


**Fig. 9.** PCA scree plot of the percentage of the variance contributed by each PC.

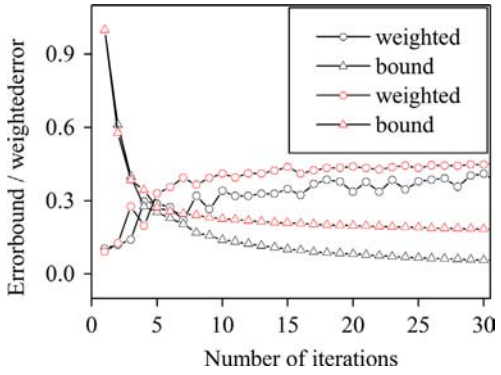


**Fig. 10.** Error bound and weighted error during Adaboost training iterations with mean centre (black) and auto scaling (red). (For interpretation of the references to color in this figure legend, the reader is referred to the web version of this article.)

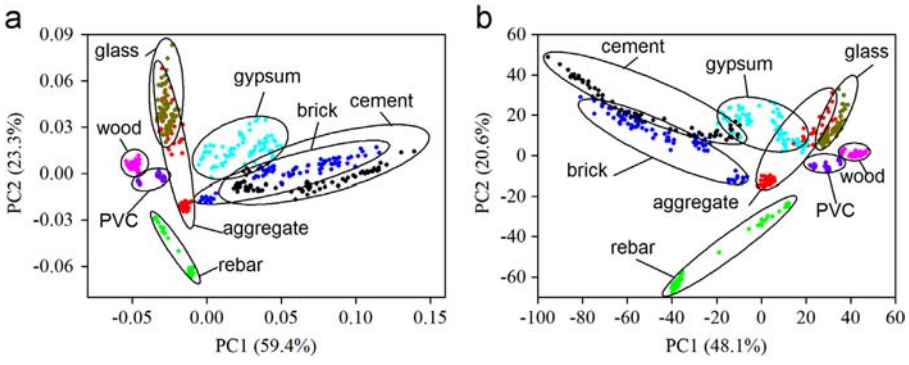


**Fig. 8.** Clusters produced by PCA using the first two PC scores. Indicated in the axis label is the PC contribution to the total variance. (a) With mean centre. (b) With auto scaling.

Since Adaboost is little susceptible to over-fitting, the first 100 PC scores from the PCA algorithm were used as input features, which proved to include all the relevant PC scores as determined by Adaboost. The one-against-all approach was applied, meaning that each single target material class is determined against the second class, which is the mix containing the other seven waste materials. Fig. 10 shows the error bound and weighted error as a function of the number of weak classifiers/iterations using both mean centre and auto scaling. It proves the error bound decreases sharply up to the first ten iterations, after which it declines quite slowly. At the point of loss of convergence the weighted error begins to fluctuate, which indicates that the following weak classifiers perform poorly and one should stop the iteration. The first few weak classifiers are the most distinctive for classification. Mean centre again outperforms auto scaling in terms of lower error bounds and weighted errors.

Table 2 lists the number of misclassifications using a training set of 72 spectra and a test set of 18 spectra per material. The relevant PC numbers for each target material were determined by Adaboost. It shows that at most 7 out of 100 PC scores actually contribute to the classification. Using mean centre, the rebar, gypsum, wood, PVC and glass were fully classified. Five spectra were not classified correctly, meaning the target material was misclassified as the mix. Using auto scaling the cement, rebar, gypsum and wood were fully classified. In total, twenty five spectra were not classified correctly. The mean centre approach outperformed auto scaling in terms of total misclassifications and is preferred for PCA–Adaboost.

Fig. 11 shows the typical erratic class boundaries produced by Adaboost, in this case for cement against the mix of other materials. For scores PC1 and PC2 the boundary 'surgically' isolates the cement, which explains the success of boosting in producing class boundaries. The inset of Fig. 11 details the class boundary in the space spanned by scores PC1 and PC5, where PC5 contributes less than 5% in the variance coverage. This inset shows that the level of PCA variance coverage has no real bearing on the performance of Adaboost.

Based on the results in Table 2, a PCA loading plot with the most distinctive PC loading vectors is shown in Fig. 12. The parts corresponding to the emission lines and bands mainly responsible for classification of the target material are marked. Rebar was best classified by PC2 in relation to Fe emissions in the UV range, while aggregates were most distinguishable with PC7 due to the Mg, Al and Li emission lines. Brick was most distinguishable with PC4 due to strong Si and Ti emission lines and emission bands.

### 3.4. Single-shot LIBS

The PLS-DA algorithm is preferred when dealing with LIBS spectra from building waste materials. In view of the envisioned application of the proposed methodology, the characterisation on the basis of single-shot spectra is highly preferred [27]. First, because averaging lowers the effective sampling and pulsed lasers with high repetition rates are quite costly. Second, because according to Fig. 3 some two out of three shots may not contribute to qualified spectra. Since the training set should be representative for the variance in the unknown spectra, the PLS-DA model should also be built using single-shot spectra. To stay in tune with the results in Table 1, we applied 720 single-shot spectra per material for the training set and 180 for the test set.

To gain some insight into the relation between the occurring spread in the raw data sets for the different materials and the robustness of PLS-DA, it is instructive to calculate the relation between the average misclassification rate, data averaging and number of PC required to achieve optimal convergence during 9-fold cross-validation for the training process. Fig. 13a shows the average misclassification rate in RMSECV as a function of PC for

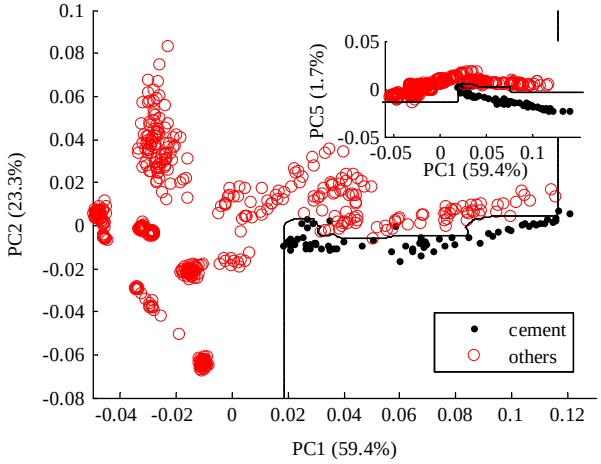


**Fig. 11.** Adaboost binary class boundaries for cement against the mix of seven other materials for training. The erratic boundary is for PC scores with high variance coverage and the inset shows a boundary with much smaller variance coverage.

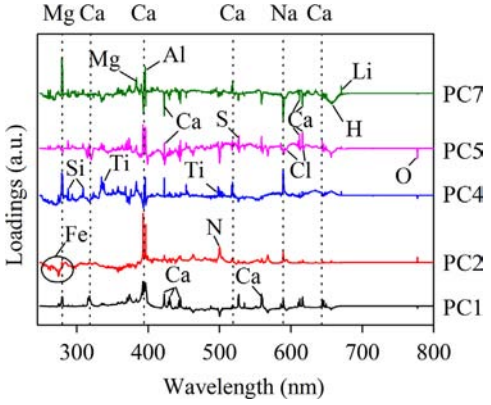


**Fig. 12.** PCA loading plot linking the dominant loading vectors to the physical spectra.

**Table 2**
PCA-PC used in Adaboost (one-against-all) during training of 72 spectra and number of misclassifications during testing of 18 spectra. Top two rows relate to mean centre (MC) and two bottom rows to auto scaling (AS). The most distinguishing PC number for the material is in bold face.

| | Cement | Aggregate | Rebar | Brick | Gypsum | Wood | PVC | Glass |
|---|---|---|---|---|---|---|---|---|
| MC | 1,2,3,**5**,10 | 1,3,**7**,8,10 | **2** | 1,3,**4** | 3,4,**5**,8 | **1** | 1,2,3,4,6,**7**,8 | **2**,3,6,10 |
| Misses | 1 | 3 | 0 | 1 | 0 | 0 | 0 | 0 |
| AS | 1,2,**6**,7 | 3,4,7,**8** | **2** | 1,4,5,**7** | **4** | **1**,9 | 1,2,3,6,9 | 1,**3**,8 |
| Misses | 0 | 6 | 0 | 1 | 0 | 0 | 1 | 17 |

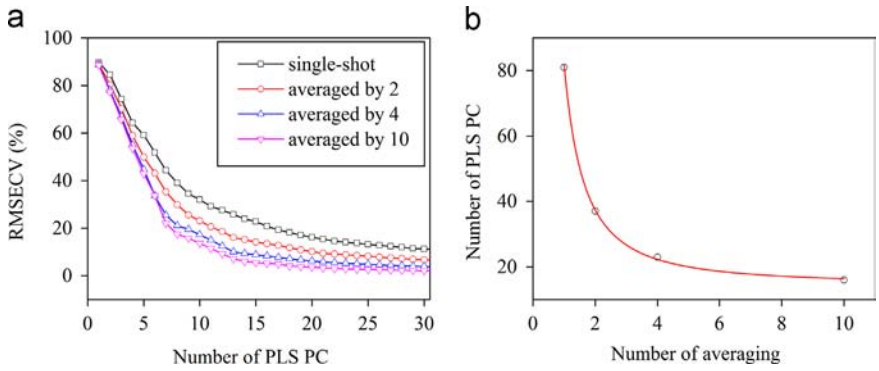


**Fig. 13.** (a) Convergence of misclassification rate in RMSECV during 9-fold cross-validation and increasing numbers of data averaging. (b) Number of PC required for less than 5.2% average misclassification rate.

**Table 3**
Misclassifications of PLS during testing of the scenarios: single-shot, 2, 4 and 10 spectra averaging with optimum number of PC, determined during training. For all materials together the number of single-shot spectra acquired was 5760 for training and 1440 for testing.

| Averaging | PC | Spectra | Cement | Aggregate | Rebar | Brick | Gypsum | Wood | PVC | Glass |
|---|---|---|---|---|---|---|---|---|---|---|
| 1 | 81 | 1440 | 0 | 3 | 0 | 1 | 0 | 0 | 0 | 0 |
| 2 | 80 | 720 | 0 | 1 | 0 | 0 | 0 | 0 | 0 | 0 |
| 4 | 74 | 360 | 0 | 0 | 0 | 0 | 0 | 0 | 0 | 2 |
| 10 | 59 | 144 | 0 | 0 | 0 | 0 | 0 | 0 | 0 | 0 |

single-shot, 2, 4, and 10 times averaging of all the spectral data, while maintaining the same size ratio of 4:1 for the size of the training set and test set. Apparently, data averaging slightly increases the rate of convergence, but for single-shot and averaging by 2 the rate slows down to a crawl after 20 PC. The local minima of RMSECV for the number of averaging spectra are 5.2% (single shot, 81 PC), 3.0% (2 averaged, 80 PC), 2.0% (4 averaged, 74 PC) and 1.5% (10 averaged, 59 PC).

Fig. 13b shows the number of PC required to get below 5.2% average misclassification rate as a function of the number of averaged spectra. The fitted smooth curve is $1/N^{3/2}$, which clearly shows the rapid convergence for increasing data averaging.

For testing, the numbers of PC determined by the local minima of RMSECV during 9-fold cross-validation were used while varying the number of averaged data. Table 3 lists the classifications using PLS-DA. As a percentage of the tested data set, the misclassifications made up 0.28% (single-shot), 0.14% (2 averaged), 0.56% (4 averaged) and 0% (10 averaged).

Since perfect discrimination is achieved only for the last scenario (10 averaged), though it will keep on improving for increasing numbers of PC, it is important to distinguish between two types of misclassifications. The first is where a target material is not classified as such (false negative), and the second is the consequence, i.e., where one type of material is misclassified as another (false positive). The consequences may be most significant in case of the identification of minority particles in a waste stream if the majority particles create many false positives. For example, if aggregate or cement particles (majority of the stream) would be mistaken for pollutants (minorities).

For 4 averaged data, one glass particle was misclassified as cement and another as PVC. For 2 averaged data, one aggregate was misclassified as glass. For single-shot data, three aggregates were misclassified as cement, wood and glass, respectively, and one brick particle was misclassified as cement. Therefore, for single-shot LIBS in a future inline application, it is paramount to tailor the size and quality of the training set and the number of PC in order to minimise the chance of the significant false positives during testing.

## 4. Conclusions

Proposed is a reliable classification methodology based on the integration of the LIBS spectral emissions over a fixed time window, starting from the deployment of the laser shot. The spectra include emissions associated with all physical stages of the laser induced breakdown experiment that may all contribute discriminating information on the targeted materials. In order not to lose any of this information, no spectral background subtraction or other type of spectral filtering was applied to the raw data. This approach extends the physical information available to classification compared to conventional quantitative LIBS, which attempts to minimise spectral contributions other than the ionic–atomic emissions. Moreover, the proposed methodology does not require the material-sensitive calibration procedures or optimizations of the time window of integration. The target materials were selected from concrete demolition waste and sampled by the laser in free air. Care was taken to mimic as close as possible the operational conditions that are found above a feed conveyor belt in recycling practice. PLS-DA and the hybrid PCA–Adaboost method (one-against-all) were investigated for their ability to classify the spectra. Ten times averaged spectra were used first, for which case PLS-DA combined with the mean centre approach gave the most robust results. Continuing with PLS-DA, the relation between data averaging for an optimum number of PC, as required for convergence, was investigated up to the single-shot scenario. The achieved misclassification rates of the tested data were: 0.28% (single-shot), 0.14% (2 averaged), 0.56% (4 averaged) and 0% (10 averaged). Single-shot LIBS constitutes the most promising real-time methodology, which success depends on the quality of the training set and the implications of the possibly remaining false positives for quality inspection of the demolition concrete waste stream.

## Acknowledgement

This work is financially supported by the European Commission in the FP7 collaborative project “Advanced Technologies for the

Production of Cement and Clean Aggregates from Construction and Demolition Waste (C2CA)", Grant agreement no. 265189.

## References

[1] F.J. Fortes, J. Moros, P. Lucena, L.M. Cabalín, J.J. Laserna, Anal. Chem. 85 (2012) 640–669.
[2] F. Vidal, S. Laville, T.W. Johnston, O. Barthélemy, M. Chaker, B. Le Drogoff, J. Margot, M. Sabsabi, Spectrochim. Acta – Part B At. Spectr. 56 (2001) 973–986.
[3] A.J. Effenberger Jr, J.R. Scott, Sensors 10 (2010) 4907–4925.
[4] R.E. Russo, X. Mao, H. Liu, J. Gonzalez, S.S. Mao, Talanta 57 (2002) 425–451.
[5] M.A. Gondal, M.N. Siddiqui, J. Environ. Sci. Health – Part A Tox./Hazard. Subst. and Environ. Eng. 42 (2007) 1989–1997.
[6] M.N. Siddiqui, M.A. Gondal, M.M. Nasr, Bull. Environ. Contam. Toxicol. 83 (2009) 141–145.
[7] M. Stepputat, R. Noll, R. Miguel, VDI Berichte; issue 1667, 2002, pp. 35–40.
[8] J. Cui, H.J. Roven, Trans. Nonferrous Metals Soc. China 20 (2010) 2057–2063.
[9] G. Asimellis, N. Michos, I. Fasaki, M. Kompitsas, Spectrochim. Acta – Part B At. Spectr. 63 (2008) 1338–1343.
[10] T.M. Moskal, D.W. Hahn, Appl. Spectrosc. 56 (2002) 1337–1344.
[11] G. Wilsch, D. Schaurich, F. Weritz, H. Wiggenhauser, in: Proceedings of the International Symposium Non-Destructive Testing in Civil Engineering (NDT-CE) in Berlin, Germany, 2003.
[12] M. Raupach, in: Restoration of Buildings and Monuments, 2009, pp. 239–254, it is a conference paper in Concrete Repair, Rehabilitation and Retrofitting II; 2nd International Conference on Concrete Repair, Rehabilitation and Retrofitting, ICCRRR-2, 24-26 November 2008, Cape Town, South Africa; editors: Mark G . Alexander , Hans-Dieter Beushausen , Frank Dehn , and Pilate Moyo; publisher: CRC Press 2008; chapter 7; page 61-66; Print ISBN: 978-0-415-46850-3; eBook ISBN: 978-1-4398-2840-3.
[13] S. Beldjilali, D. Borivent, L. Mercadier, E. Mothe, G. Clair, J. Hermann, Spectrochim. Acta Part B: At. Spectrosc. 65 (2010) 727–733.
[14] S.K. Sharma, A.K. Misra, P.G. Lucey, R.C. Wiens, S.M. Clegg, Spectrochim. Acta Part A: Mol. Biomol. Spectro. 68 (2007) 1036–1045.
[15] P. Dudragne, A.J. Amouroux, Appl. Spectrosc. 52 (1998) 1321–1327.
[16] M.D. Dyar, J.M. Tucker, S. Humphries, S.M. Clegg, R.C. Wiens, M.D. Lane, Spectrochim. Acta Part B. At. Spectrosc. 66 (2011) 39–56.
[17] J.J. Remus, R.S. Harmon, R.R. Hark, G. Haverstock, D. Baron, I.K. Potter, S.K. Bristol, L.J. East, Appl. Opt. 51 (2012) B65–B73.
[18] L. Breiman, Mach. Learn. 24 (1996) 123–140.
[19] C. Tan, M. Li, X. Qin, Anal. Bioanal. Chem. 389 (2007) 667–674.
[20] K. Watanabe, T. Iguchi, Appl. Phys. A 69 (1999) S845–S848.
[21] S. Gurlui, C. Focsa, IEEE Trans. Plasma Sci. 39 (2011) 2820–2821.
[22] M. Cirisan, J. Jouvard, L. Lavisse, L. Hallo, R. Oltra, J. Appl. Phys. 109 (2011) 103301.
[23] J.P. Singh, S.N. Thakur, Laser-Induced Breakdown Spectroscopy, 1st ed., Elsevier, Amsterdam, 2007.
[24] S. de Jong, Chemom. Intell. Lab. Syst. 18 (1993) 251–263.
[25] Y. Freund, R.E. Schapire, J Comput. Syst. Sci. 55 (1997) 119–139.
[26] M.I. Schlesinger, V. Hlavac, V. Franc, in, ⟨http://cmp.felk.cvut.cz/cmp/software/stprtool/index.html⟩, 2008.
[27] A.P.M. Michel, Spectrochim. Acta – Part B: At. Spectr. 65 (2010) 185–191.